Journal of
Applied Crystallography
ISSN 0021-8898

Received 14 August 2006
Accepted 24 November 2006

The new V12 ultra-small-angle neutron scattering and tomography instrument at the Hahn–Meitner Institut

M. Strobl,[a,b]* W. Treimer,[a,b] C. Ritzoulis,[c] A. G. Wagh,[d] S. Abbas[d] and I. Manke[b]

[a]University of Applied Sciences (TFH) Berlin, Luxemburger Str. 10, 13353 Berlin, Germany, [b]Hahn–Meitner Institut Berlin, Glienickerstr. 100, 14109 Berlin, Germany, [c]Department of Chemical Engineering, Aristotle University of Thessaloniki, 54006 Thessaloniki, Greece, and [d]Solid State Physics Division, Bhabha Atomic Research Centre, Mumbai 400085, India. Correspondence e-mail: strobl@hmi.de

The new V12 instrument at the Hahn–Meitner Institute in Berlin is a multiple setup combining several techniques to investigate the internal structure of bulk samples. It consists of two double-crystal diffractometers (DCDs) and an attenuation tomography device operating with monochromatic neutrons. The three instrument parts can be used independently at the same time. The DCDs are mainly used in the ultra-small-angle neutron scattering (USANS) regime, where they overlap the accessible range of small-angle neutron scattering instruments, while tomographic methods collect real-space information on a macroscopic scale. Together they enable structural investigations over six orders of magnitude (50 nm to 5 cm). Scattering and tomographic methods can even be combined by means of diffraction and scattering-enhanced imaging. The sample environment can be varied over a large range of temperatures and pressures for USANS measurements and a polarized USANS option is available.

1. Introduction

The recently rebuilt V12 instrument consists of three independent instrument parts operated with cold neutrons. These are: one bent-crystal-type double-crystal diffractometer (DCD), one high-resolution DCD with a flexible Bonse–Hart (Bonse & Hart, 1965) setup and one monochromatic neutron imaging device. DCDs are well known and widely used for applications in structural investigations in the ultra-small-angle neutron scattering (USANS) regime. Their resolvable q range [with q being the modulus of the scattering vector defined by $q = (4\pi/\lambda)\sin(\theta/2)$, where θ is the scattering angle and λ the wavelength] between 10^{-4} nm^{-1} and 10^{-1} nm^{-1} overlaps and extends the range of small-angle neutron scattering (SANS) instruments and enables structures from about 50 nm to 50 µm (Schaefer & Agamalian, 2004; Hainbuchner *et al.*, 2000) to be resolved. As the resolvable structures accessed by tomographic techniques reach down to a few micrometres for X-rays (Baruchel *et al.*, 2002) and to nearly 100 µm for neutrons (Schillinger *et al.*, 2000), DCDs are able to link the microscopic resolution of SANS and the macroscopic resolution of tomography. Additionally, it was demonstrated recently that the information gained by a DCD in q space combined with real-space tomographic scanning provides two additional contrast signals for tomographic imaging (Strobl, 2003; Treimer *et al.*, 2003; Strobl *et al.*, 2004*b*). By applying phase retrieval to diffraction-enhanced imaging (Podurets *et al.*, 1989) and using the filtered back projection (FBP) algorithm, the refractive index distribution in bulk samples can be reconstructed three-dimensionally. Taking into account the USANS signal in a tomographic scan, the distribution of microscopic and mesoscopic structures such as grains or pores can be reconstructed tomographically and hence spatially localized.

The monochromatic tomography setup included at V12 exploits an intense monochromatic beam for conventional attenuation contrast tomography. The monochromatic beam has the advantage of avoiding beam hardening effects, which can introduce artifacts. Hence the monochromatic beam can increase the sensitivity of imaging. Furthermore, no Bragg scattering from crystalline materials contaminates the recorded images, especially for the long wavelength of 0.52 nm used. As such scattering and beam hardening are main reasons hindering reliable quantification in neutron imaging using broad energy spectra, monochromatic imaging enables straightforward quantification in many cases without using the sophisticated and resource demanding correction algorithms currently under development (Hassanein *et al.*, 2006).

2. The instrument

The instrument uses two different monochromators placed in the neutron guide NL3b behind the cold source of the BERII research reactor at the Hahn–Meitner Institute (HMI) (Fig. 1). An asymmetric (asymmetry angle $\alpha = 41^\circ$) perfect Si [111] single-crystal monochromator provides neutrons of wavelength 4.76 (2) Å for the V12a bent-crystal-type DCD (Eichhorn, 1988; Popovic *et al.*, 1987). The analyzer is completely asymmetric (Si[111]) and can be bent to radii down to 13 m in order to tune the resolution and resolvable q range (up to $q_{max} = 10^{-1}$ nm^{-1}). The flux at the sample position is about 3×10^3 cm^{-2}s^{-1} and hence increased due to the geometry of the asymmetric reflection at the monochromator by a factor of 4 compared with the former setup at maximum resolution (Strobl *et al.*, 2006). The available beam cross section is limited by the analyzer and detector geometry to 3×20 mm^2. The resolution on the other hand is slightly decreased as the full width at half maximum (FWHM) of the instrumental curve is 7.7×10^{-4} nm^{-1}, *i.e.* doubled due to the asymmetric monochromator. The resolution loss due to putting more

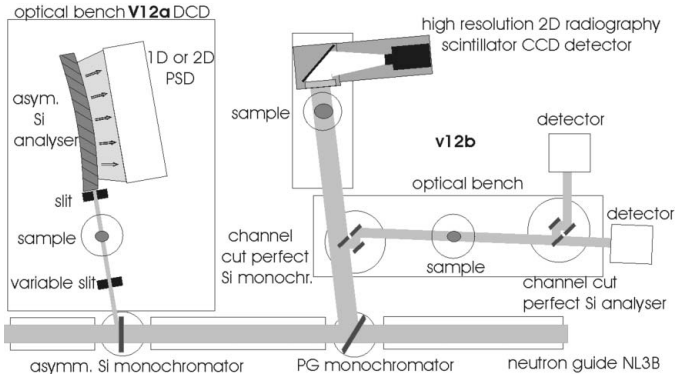

Figure 1
A schematic sketch of the V12 instrument setup.

emphasis on tomographic and medium resolution for this DCD is acceptable because the flexible second V12b DCD that can be equipped with different pairs of crystals and a special technique to tune the resolution function (Treimer *et al.*, 2001) provides ultra high resolution for special applications. The one-dimensional position sensitive detector (ORDELA 1250N, ^{3}He) is to be replaced (December 2006) by a two-dimensional PSD (DENEX-200TN, ^{3}He) in order to enable spatial resolution of the height of the sample if required for USANS or for three-dimensional tomographic reconstruction from tomographic scans (Strobl *et al.*, 2004*a*). The sample space was designed in a way that enables the use of some of the standard sample environment equipment of the Berlin Neutron Scattering Centre (BENSC), *e.g.* an orange standard cryostat (OS), an orange furnace (OF) or a closed cycle (CC) refrigerator including pressure cells and gas adsorption cells (see http://www.hmi.de/bensc/sample-env/index_en.html). Using these, a temperature range from 1.5 to 600 K and pressures up to several kbar are accessible. This option has recently been tested successfully for the gas adsorption cell.

A pyrolytic graphite [002] crystal downstream from the V12a monochromator (about 1.5 m) provides neutrons for the V12b DCD and the tomography setup. Due to the lower energy resolution of the graphite crystal and the alignment needed to provide the maximum flux wavelength of the spectrum in this guide [5.2 (1) Å], the available flux density for tomography is about 2×10^5 cm^{-2} s^{-1} at the maximum of the beam cross section of 6×6 cm^2 for imaging. The radiography and tomography position consists of an automatic sample manipulation table and a state-of-the-art two-dimensional scintillator CCD detector system (BC-704, ANDOR DV434). The spatial resolution was measured as 300 µm.

The perfect single-crystal Si [111] monochromator of the V12b DCD, which is aligned nearly perpendicular to the tomography setup, takes out less than 0.1% (5×10^2 cm^{-2} s^{-1}) of highly monochromatic neutrons from the beam between the graphite and the tomography sample position. This is an increase of flux density in the new V12b DCD of a factor of about 3. The setup can be equipped with pairs of perfect Si [111] crystals of different layouts (Agamalian *et al.*, 1997; Villa *et al.*, 2003). At the moment, crystals from single plates to seven-bounce channel-cut geometries are available. These can be used for different special applications (Treimer *et al.*, 2002; Wagh *et al.*, 2001, 2004) and in the sevenfold reflection an insert can be used to achieve the highest USANS resolution currently available, which is better than 7×10^{-5} nm^{-1} (Treimer *et al.*, 2001). Due to the instrumental layout and an additional beam shutter between the V12b DCD and the tomography setup, all parts of the instrument can be operated simultaneously and independently.

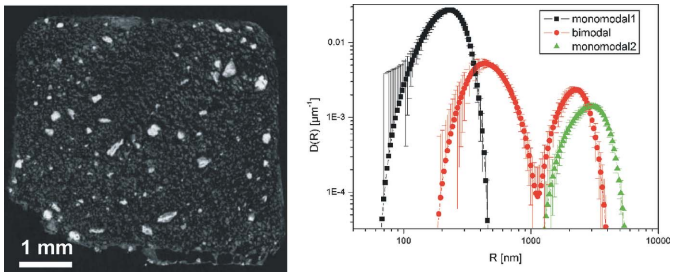

Figure 2
Left: a slice of an X-ray tomograph. Right: size distributions of various samples of porous hydroxyapatite–polymer samples.

3. Measurements

Out of various measurements and applications possible, one example realized since the new instrument started operation in mid-2005 shall be presented for every part of the instrument. At the V12a DCD the porosity of hydroxyapatite–polymer materials which are promising as bone substitutes was investigated by USANS measurements. Hydroxyapatite [$Ca_{10}(PO_4)_6(OH)_2$] is a brittle ceramic that needs mechanical reinforcement in order to cope with the stress related to the normal function of bone (Suchanek & Yoshimura, 1998). The challenge is to render these materials porous in a controlled manner. This is achieved through the templating of emulsion droplets of known size distributions into a solid matrix, followed by their elution and subsequent creation of micropores (Ritzoulis *et al.*, 2004). The porosity of such materials is crucial for the development of bone after implementation of the artificial substitute. Bimodal systems are of special interest as different pore sizes are needed with respect to hosting osteoblasts (bone-cell builders) on the one hand and to enhance their attachment by smaller pores on the other hand. USANS measurements have been utilized to probe the size distribution of the small pores in the range 0.1 to 6 µm. X-ray tomography is also being used to probe pore sizes beyond the upper limit of the USANS range, *i.e.* pore sizes of 10 to about 100 µm. Fig. 2 displays both results from USANS coupled with tomography measurements. Comparison of such results with those obtained through scanning electron microscopy (Ritzoulis *et al.*, 2004) and light scattering data of the templating droplets confirm that the pore size can be controlled by means of controlling emulsion droplet sizes, thus producing custom-built microporous materials.

The high resolution DCD V12b was used to measure the deviation of the refraction angle at a crystal prism due to dynamic diffraction when the incident beam approaches the Bragg angle. The neutron deflection δ_{cr} produced by a single-crystal prism varies markedly across a Bragg reflection (Wagh, 1987; Abbas & Wagh, 2005) from its off-reflection value δ_{am}. The extremely sharp and narrow neutron angular profile attained at the tuned Bonse–Hart setup (Treimer *et al.*, 2001) enabled a measurement of the δ_{cr} variation, in the arcsecond domain, for neutrons of wavelength 5.24 Å produced by single-crystal silicon prisms in symmetric/asymmetric {111} Bragg configurations. Each prism was mounted on a precision goniometer at the sample position and its Bragg reflection was located using an additional detector. At each angular setting of the prism within the Bragg scan, the analyser rocking curve measured the prism deflection as well as the neutron intensity transmitted by the prism. A part of the neutron beam passed directly to the analyser to provide a precise reference for the angle of incidence. The observations agree well with theory. Fig. 3 depicts a representative result obtained for a prism with an asymmetry angle of 35.3° and apex angle of 94°.

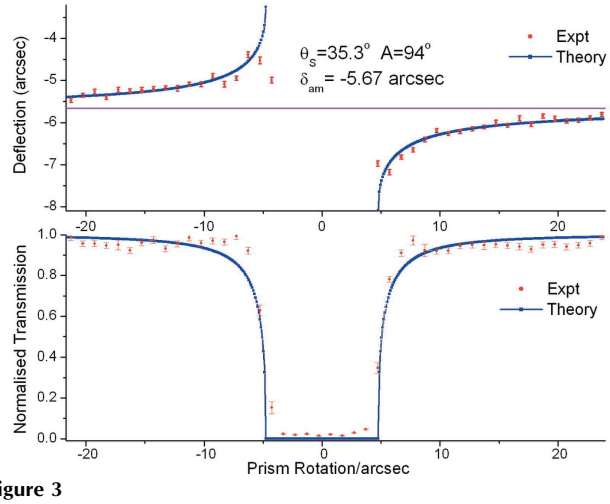

Figure 3
Refraction angle and transmitted intensity of a beam passing an Si perfect crystal wedge.

First measurements at the V12c monochromatic imaging beam have been recorded with a preliminary setup. The beam path after the monochromator could be extended to approximately 2 m. However, the resolution could not be increased significantly and is limited by the scintillator screen and the light optics, which can still be improved. The high sensitivity due to the absence of beam hardening and coherent scattering effects has been demonstrated before by quantitative tomographic measurements (Strobl *et al.*, 2006). An example of the application of such increased sensitivity is the tomogram presented in Fig. 4. It is a tomographic investigation of the distribution of soot particles in a soot particle filter. The dimensions of the industrially produced sample are 50 × 50 × 150 mm. The imaged area is restricted by the beam cross section to a height of 60 mm. It is a SiC matrix with a regular pattern of channels open only either on the upper or lower squared side. Four times 300 projection images were recorded over a range of 180°. The exposure time per image was 70 s resulting in 2 days for recording the whole tomogram. The reconstruction was performed straightforwardly using the FBP algorithm and involving only standard corrections like flat field and background corrections.

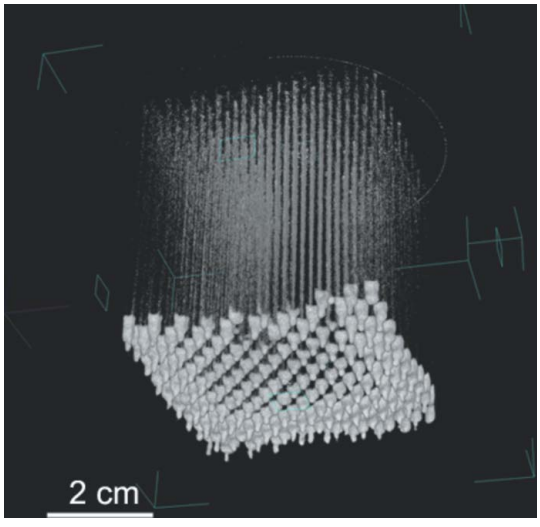

Figure 4
Image of a tomographic reconstruction of a loaded soot particle filter. Grey values corresponding to the filter material have been disabled.

In the reconstruction shown, the filter itself is made invisible by setting a limit for the displayed grey levels, *i.e.* reconstructed attenuation coefficients. The result looks promising, but due to the limited spatial resolution it is not very reliable yet. This means that agglomerates can be identified easily at the ends of the channels, where they can also be found with conventional tomography. However, the distribution of interest is the one in the walls of the filter. In the given representation it seems to be visible (upper part of Fig. 4), but the resolution is too low yet to reliably prove the information content of only a few pixels over the rather small wall thickness of the order of millimetres. Further measurements to prove the results indicated by this measurement are scheduled.

4. Conclusion

This unique combination of instruments offers a wide range of resolvable sizes from 50 nm to 5 cm, and hence covers six orders of magnitude by a combination of *q*-space and real-space resolution. It offers a fast medium resolution DCD as well as the highest resolution DCD for USANS and special applications. Additional unique features of the instrument are the option of using standard sample environment equipment in USANS measurements, a polarized beam for USANS, monochromatic neutrons for tomography and very soon a position sensitive detector for spatially resolved USANS, three-dimensional refraction and USANS contrast tomography.

This work was supported by the BMBF project 03TRTFH and the Greek project Pythagoras (EPEAEK II)/YPEPTH.

References

Abbas, S. & Wagh, A. G. (2005). *Solid State Phys. (India)*, **50**, 317–318.
Agamalian, M., Wignall, G. D. & Triolo, R. (1997). *J. Appl. Cryst.* **30**, 345–352.
Baruchel, J., Cloetens, P., Härtwig, J. & Schlenker M. (2002). *Imaging with Third Generation Synchrotron X-ray Sources*. In *Third-Generation Hard X-ray Synchrotron Radiation Sources*, edited by D. M. Mills. New York: Wiley.
Bonse, U. & Hart, M. (1965). *Appl. Phys. Lett.* **6**, 155–156.
Eichhorn, F. (1988). *Physica B*, **151**, 140–146.
Hainbuchner, M., Villa, M., Kroupa, G., Bruckner, G., Baron, M., Amenitsch, H., Seidl, E. & Rauch, H. (2000). *J. Appl. Cryst.* **33**, 851–854.
Hassanein, R., de Beer, F., Kardjilov, N. & Lehmann, E. (2006). *Physica B*, **385–386**, 1194–1196.
Podurets, K. M., Somenkov, V. A. & Shil'shtein, S. Sh. (1989). *Physica B*, **156–157**, 691–693.
Popovic, M., Stoica, A. D. & Ionita, I. (1987). *J. Appl. Cryst.* **20**, 90–101.
Ritzoulis, C., Scoutaris, N., Papademetriou, K., Kokkou, S., Stavroulias, S. & Panayiotou, C. (2004). *J. Biomed. Mater. Res. A*, **71**, 675–684.
Schaefer, D. W. & Agamalian, M. (2004). *Curr. Opin. Solid State Mater. Sci.* **8**, 39–47.
Schillinger, B., Lehmann, E. & Vontobel, P. (2000). *Physica B*, **276–278**, 59–62.
Strobl, M. (2003). PhD thesis, Technical University Vienna, Austria.
Strobl, M., Treimer, W. & Hilger, A. (2004*a*). *Nucl. Instrum. Methods Phys. Res. B*, **222**, 653–658.
Strobl, M., Treimer, W. & Hilger, A. (2004*b*). *Appl. Phys. Lett.* **85**, 488–490.
Strobl, M., Treimer, W. & Hilger, A. (2006). *Physica B*, **385–386**, 1209–1212.
Suchanek, W. & Yoshimura, M. (1998). *J. Mater. Res.* **13**, 94–117.
Treimer, W., Strobl, M. & Hilger, A. (2001). *Phys. Lett. A*, **289**, 151–154.
Treimer, W., Strobl, M. & Hilger, A. (2002). *J. Appl. Phys. A*, **74** (Suppl.), 191–193.
Treimer, W., Strobl, M., Hilger, A., Seifert, C. & Feye-Treimer, U. (2003). *Appl. Phys. Lett.* **83**, 398–400.
Villa, M., Baron, M., Hainbuchner, M., Jericha, E., Leiner, V., Schwahn, D., Seidl, E., Stahn, J. & Rauch, H. (2003). *J. Appl. Cryst.* **36**, 769–773.
Wagh, A. G. (1987). *Phys. Lett. A*, **121**, 45–49.
Wagh, A., Rakhecha, V. C., Strobl, M. & Treimer, W. (2004). *Pramana J. Phys.* **63**, 369–373.
Wagh, A., Rakhecha, V. C. & Treimer, W. (2001). *Phys. Rev. Lett.* **87**, 125504 (1–4).